Development funds for the neutron studies. This work has also benefited from the use of facilities at the Los Alamos Neutron Scattering Center, a national user facility funded as such by the Department of Energy, Office of Basic Energy Sciences.

Supplementary Material Available: Tables of fractional coordinates, general displacement parameter expressions (U's), and complete bond distances and angles (21 pages). Ordering information is given on any current masthead page.

Metal Dependence of the Nonplanar Distortion of Octaalkyltetraphenylporphyrins

L. D. Sparks,[†,‡] C. J. Medforth,[§] M.-S. Park,[‡] J. R. Chamberlain,[†] M. R. Ondrias,[‡] M. O. Senge,[§] K. M. Smith,[*,§] and J. A. Shelnutt[*,†,‡]

Contribution from the Fuel Science Department 6211, Sandia National Laboratories, Albuquerque, New Mexico 87185, Department of Chemistry, University of New Mexico, Albuquerque, New Mexico 87131, and Department of Chemistry, University of California, Davis, California 95616. *Received May 29, 1992. Revised Manuscript Received September 30, 1992*

Abstract: The biological activity of porphyrins and related tetrapyrroles in proteins may be modulated by nonplanar conformational distortions; consequently, two aspects of nonplanarity have been investigated in the highly nonplanar octaalkyltetraphenylporphyrins (OATPPs). In the first part, the effect of the central metal ion (M = Ni(II), Co(II), Cu(II), Zn(II), Co(III), Fe(III)) on the conformation of the OATPP macrocycle has been determined. Crystallographic studies reveal that the sterically encumbered, nonplanar porphyrin 2,3,7,8,12,13,17,18-octaethyl-5,10,15,20-tetraphenylporphyrin (OETPP) remains sufficiently flexible to show a small decrease in nonplanarity for large metal ions. This decrease in nonplanarity for the OETPP metal complexes is predicted by using a molecular mechanics force field derived from structural and vibrational data for planar metalloporphyrins. A detailed analysis of the crystal structures of the Co(II) and Cu(II) complexes of OETPP reveals that the metal-dependent changes in bond lengths and bond angles are qualitatively similar to the changes observed for the OEP complexes. As the metal size increases, both OEPs and OETPPs exhibit expansion of the meso bridges (increases in the C_α–C_m bond length and the C_α–C_m–C_α bond angle) and a movement of the coordinating nitrogen atoms away from the metal atom (increases in the M–N bond length and the C_α–N–C_α bond angle and a decrease in the N–C_α bond length). Furthermore, the frequencies of several structure-sensitive Raman lines correlate with structural parameters obtained from these crystallographic studies. In the second part, a combination of molecular mechanics and INDO/CI molecular orbital calculations successfully predicts the optical spectra of a series of highly substituted OATPPs with increasing nonplanar distortion. The success of these calculations indicates the importance of including both the macrocycle conformation and the peripheral substituents in the INDO calculations.

Introduction

Interest has recently been expressed in the role of nonplanar conformational distortions in modifying the biological properties of tetrapyrroles in the photosynthetic reaction center of *Rhodopseudomonas viridis*,[1] the photosynthetic antenna system of *Prosthecochloris aestuarii*,[2] methylreductase,[3] vitamin B_{12} and B_{12}-dependent enzymes,[4] and heme proteins.[5] In this regard, some octaalkyltetraphenylporphyrins (OATPPs) (Figure 1), which are nonplanar as a result of steric crowding of the peripheral substituents, have been used as model compounds to investigate the consequences of nonplanar conformational distortions.[6-14] Also, we are interested in using these highly substituted OATPPs to tailor biomimetic catalysts with a specified function and catalytic selectivity. For example, Fe, Mn, and Ru porphyrins catalyze the oxidation of alkanes,[15-18] mimicking the function of cytochrome P_{450}. The activity of these biomimetic porphyrin catalysts is determined primarily by the choice of metal, axial ligands, the electronic properties of the porphyrin macrocycle, and steric factors such as the incorporation of a substrate binding cavity.[19]

It is our goal to design substrate binding cavities for highly substituted porphyrins by using molecular modeling methods to select suitable substituents. A carefully designed binding cavity offers several benefits, including (1) the controlled access of various molecules to the active catalytic metal center, (2) enhanced binding affinity of the porphyrin for the substrate molecule of interest, (3) the trapping of intermediates of the reaction in the cavity for recombination, and (4) the prevention of undesired side reactions and catalyst self-destruction. Catalytic function may then be fine

* To whom correspondence should be addressed.
† Sandia National Laboratories.
‡ University of New Mexico.
§ University of California.

(1) (a) Deisenhofer, J.; Michel, H. *Angew. Chem., Int. Ed. Engl.* **1989**, *28*, 829-847. (b) Deisenhofer, J.; Michel, H. *Science* **1989**, *245*, 1463-1473.
(2) Tronrud, D. E.; Schmid, M. F.; Matthews, B. W. *J. Mol. Biol.* **1986**, *188*, 443-454.
(3) (a) Furenlid, L. R.; Renner, M. W.; Smith, K. M.; Fajer, J. *J. Am. Chem. Soc.* **1990**, *112*, 1634-1635. (b) Furenlid, L. R.; Renner, M. W.; Fajer, J. *J. Am. Chem. Soc.* **1990**, *112*, 8987-8989.
(4) Geno, M. K.; Halpern, J. *J. Am. Chem. Soc.* **1987**, *109*, 1238-1240.
(5) Alden, R. G.; Ondrias, M. R.; Shelnutt, J. A. *J. Am. Chem. Soc.* **1990**, *112*, 691-697.
(6) Barkigia, K. M.; Chantranupong, L.; Smith, K. M.; Fajer, J. *J. Am. Chem. Soc.* **1988**, *110*, 7566-7567.
(7) Barkigia, K. M.; Berber, M. D.; Fajer, J.; Medforth, C. J.; Renner, M. W.; Smith, K. M. *J. Am. Chem. Soc.* **1990**, *112*, 8851-8857.
(8) Renner, M. W.; Cheng, R.-J.; Chang, C. K.; Fajer, J. *J. Phys. Chem.* **1990**, *94*, 8508-8511.
(9) Medforth, C. J.; Berber, M. D.; Smith, K. M.; Shelnutt, J. A. *Tetrahedron Lett.* **1990**, *31*, 3719-3722.
(10) Shelnutt, J. A.; Medforth, C. J.; Berber, M. D.; Barkigia, K. M.; Smith, K. M. *J. Am. Chem. Soc.* **1991**, *113*, 4077-4087. The functional form used for the inversion energy was stated to be quadratic in the distortion angle, ω. Actually, a $1 - \cos\omega$ functional form was employed. The force constant for Ni inversion is zero and not 35 given in the original reference.
(11) Medforth, C. J.; Smith, K. M. *Tetrahedron Lett.* **1990**, *31*, 5583-5586.
(12) The nickel complex of porphyrin **4** could not be crystallized due to its poor solubility. The nickel complex of porphyrin **7** crystallizes in two conformations which are more akin to the crystal structure of tetragonal NiOEP ((a) Meyer, E. F. *Acta Crystallogr.* **1972**, *B28*, 2162-2167. (b) Cullen, D. L.; Meyer, E. F., Jr. *J. Am. Chem. Soc.* **1974**, *96*, 2095-2102) rather than the very nonplanar saddle conformations seen for the other nickel OATPPs. The copper complex of porphyrin **8** is essentially planar (Senge, M. O.; Medforth, C. J.; Sparks, L. D.; Shelnutt, J. A.; Smith, K. M. *Inorg. Chem.*, submitted).

0002-7863/93/1515-581$04.00/0

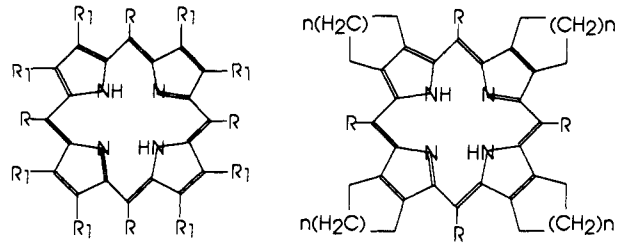

1. R = C_6H_5 R_1 = CH_3 (OMTPP)
2. R = C_6H_5 R_1 = CH_2CH_3 (OETPP)
3. R = C_6H_5 R_1 = $CH_2CH_2CH_3$ (OPTPP)
4. R = R_1 = C_6H_5 (DPP)

5. n = 1 R = C_6H_5 (TC_5TPP)
6. n = 2 R = C_6H_5 (TC_6TPP)
7. n = 3 R = C_6H_5 (TC_7TPP)
8. n = 1 R = $C_6H_2(3,4,5\text{-}OCH_3)$ ($TC_5T(OMe)_3PP$)
9. n = 1 R = $(CH_2)_4CH_3$ (TC_5TC_5P)
10. n = 1 R = CH_2CH_3 (TC_5TC_2P)

Figure 1. Structures of the series of octaalkyl(aryl)tetraaryl(alkyl)-porphyrins discussed in the text.

tuned by varying the pocket's size, shape, hydrophobicity, cavity rigidity, and the charges of the groups lining the pocket.

Some of the highly substituted metalloporphyrins such as the nickel(II) complex of OPTPP (**3**, Figure 1) possess binding cavities that can accommodate small molecules. Thus, it is of interest to determine the effects of incorporation of progressively larger metal atoms on the planarity of the porphyrin macrocycle and the consequent effect on the size and shape of the binding pocket. We also wished to determine the effects of nonplanarity on the electronic states of the porphyrin macrocycle, since changes in the electronic structure might influence catalytic activity.

There is now a considerable body of information describing the structural and spectroscopic properties of highly nonplanar OATPPs.[6-14] The crystal structure[7] of the zinc(II) complex of OETPP (**2**) shows that the porphyrin macrocycle exists in a highly nonplanar saddle conformation;[13] and variable-temperature NMR[7,9] and resonance Raman[10,14c] studies show that a nonplanar conformation is also retained in solution. In agreement with INDO/CI (intermediate neglect of differential overlap with configuration interaction) molecular orbital calculations, nonplanar ZnOETPP is easier to oxidize and has an optical spectrum that is red-shifted when compared to planar porphyrins.[6] Significant differences in spin-delocalization have also been noted for a saddle-shaped porphyrin cation radical compared to a planar porphyrin cation radical.[8]

A molecular mechanics force field capable of predicting the conformations of OATPPs has been developed and tested.[9,10] On the basis of the molecular mechanics calculations, nickel(II) complexes of OMTPP (**1**), OETPP (**2**), OPTPP (**3**), tetracyclohexenyltetraphenylporphyrin (TC_6TPP, **6**), and tetracycloheptenyltetraphenylporphyrin (TC_7TPP, **7**) adopt nonplanar saddle conformations, whereas nickel(II) tetracyclopentenyltetraphenylporphyrin (TC_5TPP, **5**) was calculated to be planar. These structural predictions have been verified by subsequent crystallographic studies.[12,14] The different distortion modes (i.e. saddle vs ruffled)[13] observed in crystal structures of dodecaphenylporphyrin (DPP, **4**) and the nickel(II) complex of tetracyclopentenyltetrapentylporphyrin (TC_5TC_5P, **9**) are also correctly predicted using this molecular mechanics force field.[14b]

Correlations between nonplanarity and optical absorption and Raman spectroscopic parameters have been obtained for porphyrins **1**–**7**.[9,10] The optical spectra of porphyrins **5**–**7** show a progressive shift to absorption at lower energy as the size of the fused ring, the resulting peripheral steric strain, and, hence, the degree of nonplanarity are increased. Similarly, an increase in ΔG^* for inversion of the saddle conformation of the porphyrin macrocycle is seen as the size of the fused ring is increased.[9]

The relationships between structural parameters and the frequencies of resonance Raman lines have been investigated in detail.[10,14c] Several structural parameters of metalloporphyrins such as the metal core size,[20-22] oxidation state of the central metal[23] or the porphyrin macrocycle,[24,25] and the spin state of the metal,[26] have previously been correlated with the vibrational frequencies of the structure-sensitive modes in resonance Raman spectra. The correlation between core size and the frequencies of a group of Raman lines called the "core-size" marker lines has been used extensively. The nickel complexes of porphyrins **5**–**7** have varying degrees of nonplanarity and show a correlation between Raman frequency and core size with a slope that is positive. In contrast, a *negative* slope is seen for the mostly planar metal complexes of octaethylporphyrin (OEP) and tetraphenylporphyrin (TPP).[10] Because the core size correlates differently for the two series of porphyrins, core size is probably not a determining factor for the marker line frequencies. Instead, the similarity of the correlations with C_α–N–C_α angle, which give positive slopes for both data sets, indicates that this structural parameter may be more closely related to the marker line frequencies.

In the present study, two new aspects of porphyrin nonplanarity have been investigated. First, the structures of a series of metal complexes of OETPP (**2**) are investigated by X-ray crystallography and resonance Raman spectroscopy, with the aim of establishing how a nonplanar porphyrin adapts to changes in the size of the central metal ion. The metal dependence of the bond lengths and bond angles in both planar and nonplanar porphyrins is analyzed and the effect of metal size on the degree of distortion from planarity for a series of metal ions (M = Ni(II), Co(II), Cu(II), Zn(II), Co(III), Fe(III)) is determined. A molecular mechanics force field for nickel porphyrins described previously[10] is expanded to include these additional metal ions, and the calculated structures for the metal octaethylporphyrins (MOEPs), the metal tetraphenylporphyrins (MTPPs), and the highly nonplanar MOETPPs are compared with the structures determined crystallographically. Detailed comparisons of calculated and experimental metalloporphyrin structures validate the predictions of the molecular model. Finally, the metal dependence of the resonance Raman spectra of the nonplanar MOETPPs is compared to that of the planar MOEPs and MTPPs.

(13) The ruffled and saddle conformations are those defined by Scheidt: Scheidt, W. R.; Lee, Y. *J. Structure Bonding* **1987**, *64*, 1–70. In a saddle conformation alternate pyrrole rings are tilted up and down with respect to a least-squares plane through the 24 atoms of the porphyrin core. In a ruffled conformation alternate pyrrole rings are twisted clockwise or counterclockwise about the M–N bond such that the meso carbon atoms are alternately above or below the least-squares plane through the 24 atoms of the porphyrin core.

(14) (a) Crystal structures of the nickel complexes of porphyrins **2**, **3**, and **6** show very nonplanar saddle conformations (Barkigia, K. M.; Berber, M. D.; Fajer, J.; Furenlid, L. R.; Medforth, C. J.; Renner, M. W.; Smith, K. M., manuscript in preparation). A preliminary crystal structure of the nickel complex of porphyrin **7** also shows a nonplanar saddle conformation. (b) Medforth, C. J.; Senge, M. O.; Smith, K. M.; Sparks, L. D.; Shelnutt, J. A. *J. Am. Chem. Soc.*, in press. (c) Shelnutt, J. A.; Majumder, S. A.; Sparks, L. D.; Hobbs, J. D.; Medforth, C. J.; Senge, M. O.; Smith, K. M.; Miura, M.; Luo, L.; Quirke, J. M. E. *J. Raman Spectrosc.* **1992**, *23*, 523–529.

(15) Groves, J. T.; Nemo, T. E.; Myers, R. S. *J. Am. Chem. Soc.* **1979**, *101*, 1032–1033.

(16) (a) Smegal, J. A.; Hill, C. L. *J. Am. Chem. Soc.* **1983**, *105*, 3515–3521. (b) Wayland, B. B.; Del Rossi, K. J. *J. Organometal. Chem.* **1984**, *276*, C27–C30.

(17) (a) Tabushi, I.; Koga, N. *J. Am. Chem. Soc.* **1979**, *101*, 6456–6458. (b) de Poorter, B.; Ricci, M.; Bortolini, O.; Meunier, B. *J. Mol. Catal.* **1985**, *31*, 221–224.

(18) Belova, V. S.; Khenkin, A. M.; Shilov, A. E. *Kinet. Catal. (Engl. Transl.)* **1987**, *28*, 1017.

(19) Cook, B. R.; Reinhart, T. J.; Suslick, K. S. *J. Am. Chem. Soc.* **1986**, *108*, 7281–7786.

(20) Spaulding, L. D.; Chang, C. C.; Yu, N.-T.; Felton, R. H. *J. Am. Chem. Soc.* **1975**, *97*, 2517–2525.

(21) Stong, J. D.; Spiro, T. G.; Kubaska, R. J.; Shupack, S. I. *J. Raman Spectrosc.* **1980**, *9*, 312–314.

(22) Parthasarathi, N.; Hansen, C.; Yamaguchi, S.; Spiro, T. G. *J. Am. Chem. Soc.* **1987**, *109*, 3865–3871.

(23) Yamamoto, T.; Palmer, G.; Gill, D.; Salmeen, I. T.; Rimai, L. *J. Biol. Chem.* **1973**, *248*, 5211–5213.

(24) Ksenofontova, N. M.; Maslov, V. G.; Sidorov, A. N.; Bobovich, Ya. S. *Opt. Spectrosc. (Engl. Transl.)* **1976**, *40*, 462–465.

(25) Yamaguchi, H.; Nakano, M.; Itoh, K. *Chem. Lett.* **1982**, 1397–1400.

(26) Spiro, T. G. In *Chemical and Biochemical Applications of Lasers*; Moore, C. G., Ed.; Academic: New York, 1974; Chapter 2.

Table I. Crystallographic Data for Metal OETPP Complexes

formula	$C_{58}H_{60}N_4Co$	$C_{58}H_{60}N_4Cu$	$C_{58}H_{60}N_4Zn^a$
solvents present	$2CH_2Cl_2$	$2CH_2Cl_2$	$3CH_3OH$
crystal color	dark red	red	green
crystal shape	parallelepiped	parallelepiped	metallic plates
dimensions, mm	1.1 × 0.4 × 0.23	0.9 × 0.6 × 0.6	
crystal system	triclinic	triclinic	triclinic
space group	*P*1*bar*	*P*1*bar*	*P*1*bar*
a, Å	13.073 (4)	13.145 (4)	14.017 (10)
b, Å	13.852 (2)	13.911 (5)	16.494 (7)
c, Å	16.626 (6)	16.604 (5)	13.073 (9)
α, deg	104.22 (3)	104.35 (2)	96.12 (5)
β, deg	97.32 (3)	97.44 (2)	107.48 (6)
γ, deg	107.49 (2)	107.75 (2)	105.23 (6)
V	2716.1 (13)	2731.5 (15)	2724.5
Z	2	2	2
diffractometer	Siemens R3m/v	Siemens R3m/v	Enraf-Nonius CAD4
radiation	Mo Kα	Mo Kα	Mo Kα
temperature, K	130	130	200
scan type	Wyckoff	Wyckoff	
2θ range, deg	0–55	0–55	
no. of total reflcns	11809	12560	8029
no. of obs reflcns	7630	7018	4281
no. of parameters	651	641	
R	0.071	0.072	0.062
R_w	0.080	0.080	0.062

[a] Data from ref 7.

In the second part, we investigate the possibility of combining the molecular mechanics calculations with INDO/CI molecular orbital methods[27] for predicting the electronic states of a series of nickel porphyrins. The visible absorption spectra of the nickel complexes of porphyrins **5**, **6**, **1**, and **2** are progressively shifted to absorption at lower energy as greater steric strain is introduced at the porphyrin periphery.[9,10] It is shown that this trend can be readily reproduced if the macrocycle conformation predicted by molecular mechanics calculations is used in the INDO/CI calculations. In addition, *all* of the peripheral substituents must be included in the INDO/CI calculations to obtain good agreement with the UV–visible absorption spectra.

Materials and Methods

Synthesis and Characterization of Porphyrins. Free base OETPP was synthesized using the procedure described previously[7] and Co(II) and Cu(II) complexes were prepared using the metal acetate method.[28] The metalloporphyrins were recrystallized from dichloromethane by addition of methanol. Optical data (λ_{max}) for the B (Soret) and Q (β and α) bands for these porphyrins are as follows: CoOETPP, 432, 554, 578 nm; CuOETPP, 430, 568, 598 nm. The proton NMR spectrum of CoOETPP confirmed the presence of a low-spin Co(II) ion complexed to the porphyrin. Proton NMR for CoOETPP in $CDCl_3$ consists of the following peaks (br = broad, t = triplet, d = doublet): 16.20 (br, 8H, ortho phenyl), 10.46 (br, 8H, meta phenyl), 10.22 (t, 4H, para phenyl), 8.01 and 5.28 (br, 8H each, CH_2), 0.20 (br, 24H, CH_3). The preparation of Ni^{II}OETPP and $Zn^{II}(CH_3OH)$OETPP has been described previously.[7,10]

The bis-pyridine Co(III) complex of OETPP was prepared by refluxing a solution of CoOETPP in dichloromethane with a large excess of pyridine for 12 h. The reaction mixture was washed several times with water, the organic layer was separated and dried by filtration through anhydrous sodium sulfate, and the solvent was removed under vacuum. The residue was purified by precipitation from dichloromethane using hexane. Optical data (λ_{max}) for $Co^{III}(py)_2$OETPP: 466, 580, 624 nm. Proton NMR for $Co^{III}(py)_2$OETPP ($CDCl_3$): 8.15 (d, 8H, ortho phenyl), 7.67 (t, 8H, metal phenyl), 7.73 (t, 4H, para phenyl), 2.21 (br, 16H, CH_2), −0.05 (t, 24H, CH_3), 6.22 (t, 2H, para pyridine), 5.28 (t, 4H, meta pyridine), 2.49 (d, 4H, ortho pyridine). The identity of the anion in the complex is unknown. Attempts to grow crystals of this complex were unsuccessful.

Fe^{III}(Cl)OETPP was prepared as follows. OETPP was dissolved in dimethylformamide and the mixture deoxygenated by stirring at 150 °C under a flow of nitrogen for 15 min. Iron(II) chloride tetrahydrate (1 g) was added all at once to the reaction mixture which rapidly changed from the dark green color of the porphyrin dication to the red-brown color of the iron complex. The reaction vessel was opened to the atmosphere, refluxed for 5 min, and then allowed to cool. The reaction mixture was washed with 0.02 M HCl, the solvent was removed under vacuum, and the resulting residue was purified using a Brockman Grade III alumina column with 0.5% methanol in dichloromethane as eluent. The red-brown band of iron porphyrin eluted rapidly and was collected and washed with 0.02 M HCl and the solvent was removed under vacuum. The proton NMR spectrum of Fe(Cl)OETPP confirmed the presence of the high-spin Fe(III) ion. Proton NMR for Fe^{III}(Cl)OETPP (CD_2Cl_2): 10.8, 8.2 (br, 4H each, ortho phenyl), 13.1, 12.9 (br, 4H each, meta phenyl), 7.1 (br, 4H, para phenyl), 45.6, 38.7, 35.7, 24.2 (br, 4H each, CH_2), 3.7, 1.4 (br, 12H each, CH_3). The optical spectrum of Fe(Cl)-OETPP shows a split Soret band (399 and 442 nm) and several poorly resolved bands in the 500–650 nm region of the spectrum. No attempts were made to grow crystals of Fe(Cl)OETPP.

Proton NMR spectra were recorded at a frequency of 300 MHz and at ambient temperature. Optical spectra were recorded on a Hewlett Packard 8450A spectrophotometer using dichloromethane as solvent.

Crystal Structure Determinations. Crystals of Co^{II}OETPP and Cu^{II}OETPP suitable for structure determinations were grown by slow diffusion of methanol into a solution of the metalloporphyrin in dichloromethane. The crystal structure of Co^{II}OETPP was solved by direct methods using the SHELXTL PLUS package and refined using a full-matrix least-squares procedure.[29a] The CuOETPP structure was solved by a Patterson synthesis using the SHELXTL PLUS package and was also refined using a full-matrix least-squares procedure.[29a] The CuOETPP data was corrected for absorption.[29b] In both cases the hydrogen atoms were refined using a rigid model and a fixed isotropic *U* value. The non-hydrogen atoms were refined anisotropically. Crystallographic data for Co^{II}OETPP and Cu^{II}OETPP are given in Table I together with crystallographic data for $Zn^{II}(CH_3OH)$OETPP.[7]

Resonance Raman Spectroscopic Studies. Resonance Raman spectra were obtained using the 413.1-nm line from a Krypton ion laser (Coherent, Inc.) as the excitation source. The scattered light was collected at 90° to the direction of propagation and polarization of the exciting laser light. For solution spectra, the metalloporphyrins were dissolved in carbon disulfide and ~150-μL aliquots were added to each side of a two-compartment Raman cell. Laser power was typically ~100 mW at the sample and sample concentrations were in the range 1×10^{-4} to 1×10^{-5} M. NiOETPP was added to the reference chamber and resonance

(27) (a) Pople, J. A.; Beveridge, D. L.; Dobosch, P. *J. Chem. Phys.* **1967**, *47*, 2026–2033. (b) Ridley, J. E.; Zerner, M. C. *Theor. Chim. Acta* **1973**, *32*, 111–134. (c) Zerner, M. C.; Loew, G. H.; Kirchner, R. F.; Mueller-Westerhoff, U. T. *J. Am. Chem. Soc.* **1980**, *102*, 589–599. (d) Edwards, W. D.; Weiner, B.; Zerner, M. C. *J. Phys. Chem.* **1988**, *92*, 6188–6197. (e) Bacon, A. D.; Zerner, M. C. *Theor. Chim. Acta* **1979**, *53*, 21–54.

(28) Buchler, J. W. In *Porphyrins and Metalloporphyrins*; Smith, K. M., Ed.; Elsevier: Amsterdam, 1975; Chapter 5.

(29) (a) Program SHELXTL-PLUS for crystal structure solution: Sheldrick, G. M., Universitat Gottingen, Germany, 1989. (b) The program XABS (Hope, H.; Moezzi, B., 1987, University of California, Davis) was used to obtain an absorption tensor from $F_o - F_c$ differences.

Table II. Metal Parameters Used in Molecular Mechanics Calculations

metal	R_{eq}[a]	R_{nb}[b]	mass
Ni(II)	1.855	2.27	58.700
Co(II)	1.930	3.40	58.933
Cu(II)	1.970	3.40	63.546
Zn(II)	2.070	4.54	65.380
Co(III)	1.900	3.40	58.933
Fe(III)	1.975	4.54	55.847

[a] The equilibrium bond distance of the M-N bond. [b] The homonuclear bond separation of the M-N bond. Values interpolated from parameters given in ref 33.

Raman spectra of pairs of MOETPPs were obtained simultaneously using a dual-channel Raman spectrometer described elsewhere.[30] Frequencies were obtained from the peak positions of the lines in fast-Fourier-transform smoothed spectra.

The Raman cell was rotated at 50 Hz to prevent sample heating. Sample integrity was monitored by UV-visible absorption spectroscopy before and after the Raman spectrum was obtained and by examination of individual half-hour scans of the Raman spectrum. Porphyrin photodegradation was not noted during the five to ten 30-min scans required to obtain spectra for the Ni(II), Co(II), Cu(II), and Fe(III) complexes. However, the CS_2 solution spectrum of $Zn^{II}(CH_3OH)$OETPP consists of the sum of only two scans obtained prior to significant photodegradation. The Raman spectrum of $Co^{III}(py)_2$OETPP was obtained in CS_2 with excess pyridine added to insure total ligation. A photochemical change was noted for this sample after about 2 h in the laser beam. However, the Raman spectrum (not shown) was easily obtained prior to the onset of photochemistry. To determine the nature of the photochemical process, a sample was irradiated for a long period of time and an absorption spectrum was taken after exposure. The post-Raman absorption spectrum was nearly identical with that of Co^{II}OETPP, suggesting that slow photoreduction occurred.

For Raman spectra of polycrystalline samples, the spectrometer was used in the conventional single-channel mode. Spectra were obtained using less than 10 mW of 413.1-nm radiation. No sample degradation was evident for Ni^{II}-, Co^{II}-, and Cu^{II}OETPP upon examination of 15-20 sequential half-hour scans. However, the polycrystalline Raman spectra of $Zn^{II}(CH_3OH)$OETPP and $Fe^{III}(Cl)$OETPP (not shown) were of poor quality as a result of photodecomposition of the sample in the laser beam.

Molecular Mechanics Calculations. Molecular mechanics calculations were performed using BIOGRAF software (Molecular Simulations, Inc.) and a force field for porphyrins developed previously.[10] The force field is based on a recent NiOEP normal coordinate analysis[31] and the crystal structure of planar triclinic B NiOEP.[32] Parameters for the new metals given in Table II were obtained by changing the equilibrium M-N bond distance (R_{eq}), the homonuclear nonbond separation (R_{nb}), and the atomic mass. The atomic mass was set to the natural abundance value and R_{nb} was obtained from the DREIDING force field,[33] or in the cases of Co(II), Co(III), and Cu(II), values for R_{nb} were obtained by interpolation between the DREIDING values for Ni (2.27 Å) and the values for Fe(II) and Zn(II) (4.54 Å). A Lennard-Jones 12-6 potential was used for the van der Waals interactions for all atoms. A cutoff distance of 9 Å and a switching function[10,33] were used for the nonbonding energy term. Interactions between bonded atoms (1,2 interactions) and atoms involved in angle interactions (1,3 interactions) were neglected. For all metals, the M-N force constant and the depth of the Lennard-Jones 12-6 potential well were left at the nickel values. Also, parameters for torsions, inversions, and bond angle bends involving the metal atom remained as reported previously for nickel porphyrins.[10]

With these metal parameters determined, the unconstrained equilibrium M-N bond distance R_{eq} was varied until the M-N bond distance in the energy optimized structure matched the M-N bond distance observed in the crystal structure of the planar metalloporphyrin chosen as the reference structure. If axial ligands were present in the X-ray structure, then they were also included in the structure that was energy optimized. The energy-optimized structure obtained using the best value for R_{eq} was then compared in detail to the X-ray crystal structure of the reference planar metalloporphyrin (vide infra). Finally, this force field was then used to calculate the structures of the nonplanar MOETPPs. For Co^{II}- and Cu^{II}OETPP, a detailed comparison with the X-ray structures was made (vide infra).

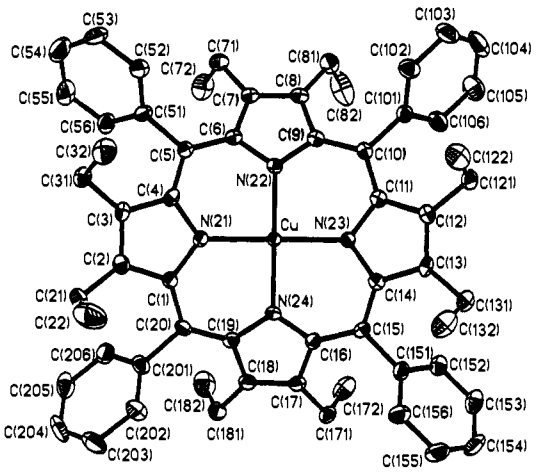

Figure 2. View of the molecular structure and numbering scheme for CuOETPP.

Because the MOETPP macrocycle is in a saddle conformation, each ethyl group can be oriented either quasi-axially or quasi-equatorially depending on the angle of rotation about the C_β-CH_2 bond. The results given are for all of the ethyl groups in quasi-axial orientations as observed in the X-ray crystal structures. However, molecular mechanics calculations for MOEPs and MOETPPs starting with other orientations of the ethyl groups give energy-optimized structures that differ in total energy. In fact, the orientation of the ethyl groups observed in the MOETPP crystal structures is *not* the conformer calculated (with this force field) to be the lowest in energy. Recently, we have found that a modified force field that, among other things, includes the electrostatic contributions to the energy successfully predicts that the all-axial conformer has the lowest energy. However, with either force field the saddle conformation of the OETPP macrocycle varies little for these different ethyl-group conformers and the previous force field is used in these calculations.

Multiple alkyl-substituent conformers have been observed for other porphyrins, including the *meso*-alkyl substituents of the nickel complexes of porphyrins 9 and **10**.[14b] In this case, the calculated energy differences of macrocycles with different quasi-axial and quasi-equatorial alkyl orientations are closer in energy and are in agreement with the relative stabilities of the conformers as determined by NMR spectroscopy. We have also investigated the axial-equatorial alkyl-group equilibrium for cobalt(II) porphyrins including CoOETPP. Proton NMR chemical shifts for the methyl protons of the ethyl groups were calculated using the Co(II) paramagnetic effect.[34a] Comparison of these calculated and observed chemical shifts suggests that the solution CoOETPP conformation is heavily biased toward the all-axial ethyl orientation.[34b]

INDO/CI Molecular Orbital Calculations. The molecular orbital (MO) calculations were performed using the intermediate neglect of differential overlap (INDO)[27] approximation with the Hartree-Fock (HF) self-consistent-field (SCF) method. The program (kindly provided by M. C. Zerner, University of Florida) was expanded to accommodate a larger basis set in order to realize the full effect of the substituents. A closed shell restricted HF operator was used for the nickel porphyrins. The SCF calculations were followed by configuration interaction (CI) calculations by using a Rumer diagram technique.[35] Each CI calculation used approximately 150-250 singly excited configurations. It has been shown that inclusions of doubly excited configurations lowers the calculated energy of the Soret band, resulting in better agreement with experimental results, but does not change the overall features of the calculated spectra.[36] The triplet spectra of NiOETPP could not be calculated with the program because too many basis functions were required.

Molecular structures for nickel complexes of porphine, TPP, OEP, **1**, **2**, **5**, and **6** were taken from the molecular mechanics calculations de-

(30) Shelnutt, J. A. *J. Phys. Chem.* **1983**, *87*, 605-616.
(31) (a) Abe, M.; Kitagawa, T.; Kyogoku, Y. *J. Chem. Phys.* **1978**, *69*, 4526-4534. (b) Li, X.-Y.; Czernuszewicz, R. S.; Kincaid, J. R.; Spiro, T. G. *J. Am. Chem. Soc.* **1989**, *111*, 7012-7023. (c) Li, X.-Y.; Czernuszewicz, R. S.; Kincaid, J. R.; Stein, P.; Spiro, T. G. *J. Phys. Chem.* **1990**, *94*, 47-61.
(32) Brennan, T. D.; Scheidt, W. R.; Shelnutt, J. A. *J. Am. Chem. Soc.* **1988**, *110*, 3919-3924.
(33) Mayo, S. L.; Olafson, B. D.; Goddard, W. A., III *J. Phys. Chem.* **1990**, *94*, 8897-8909.
(34) (a) Abraham, R. J.; Marsden, I.; Xiujing, L. *Magn. Reson. Chem.* **1990**, *28*, 1051-1057. (b) Medforth, C. J.; Sparks, L. D.; Abraham, R. J.; Smith, K. M.; Shelnutt, J. A., to be published.
(35) Reeves, C. *Commun. ACM* **1966**, *2*, 276-279.
(36) Edwards, W. D.; Weiner, B.; Zerner, M. C. *J. Am. Chem. Soc.* **1986**, *108*, 2196-2204.

Table III. Average Bond Lengths and Angles for Metal Complexes of Octaethyltetraphenylporphyrin Obtained from X-ray Crystallography

structural parameters	NiOETPP[a]	CoOETPP	CuOETPP	ZnOETPP[b] (CH_3OH)	effect of larger metal
bond lengths (Å)					
M–N	1.906 (2)	1.929 (3)	1.977 (5)	2.063 (5)	increase
$N–C_\alpha$		1.382 (6)	1.378 (8)	1.371 (2)	decrease
$C_\alpha–C_\beta$		1.457 (7)	1.458 (8)	1.461 (2)	
$C_\beta–C_\beta$	1.365 (5)	1.362 (7)	1.368 (8)	1.370 (7)	
$C_\alpha–C_m$		1.402 (7)	1.404 (8)	1.416 (3)	increase
bond angles (deg)					
N–M–N		90.5 (2)	90.3 (2)	89.4 (4)	
$M–N–C_\alpha$		125.6 (3)	124.7 (4)	122.9 (6)	decrease
$C_\alpha–N–C_\alpha$	105.9 (2)	105.6 (4)	106.6 (5)	107.7 (5)	increase
$N–C_\alpha–C_\beta$		110.0 (4)	109.6 (5)	109.2 (3)	
$C_\alpha–C_\beta–C_\beta$		106.7 (4)	107.0 (5)	106.8 (2)	
$N–C_\alpha–C_m$		121.7 (4)	122.0 (5)	122.4 (2)	
$C_\alpha–C_m–C_\alpha$		122.2 (5)	123.4 (5)	124.4 (4)	increase
$C_m–C_\alpha–C_\beta$		127.9 (5)	128.1 (5)	128.2 (2)	
pyrrole tilt[c] (deg)		27.6	27.4	27.4	
phenyl twist[d] (deg)		46.1	46.8	45.5	

[a] K. Barkigia, J. Fajer, personal communication. [b] Data from ref 7. [c] The tilt angle of the pyrrole rings is defined relative to the average plane of the 24 macrocycle atoms. [d] The phenyl twist angle is defined relative to the average plane of the 24 macrocycle atoms.

Table IV. Average Bond Lengths and Angles for Planar Metal Complexes of Octaethylporphyrin Obtained from X-ray Crystallography

structural parameters	NiOEP[a] triclinic B	CoOEP $(3MePy)_2$[b]	CuOEP[c] triclinic B	ZnOEP (py)[d]	effect of larger metal
bond lengths (Å)					
M–N	1.952 (4)	1.992 (1)	1.998 (3)	2.067 (6)	increase
$N–C_\alpha$	1.385 (6)	1.374 (3)	1.382 (5)	1.366 (1)	
$C_\alpha–C_\beta$	1.444 (8)	1.449 (2)	1.450 (6)	1.452 (6)	
$C_\beta–C_\beta$	1.332 (8)	1.355 (3)	1.347 (6)	1.353 (5)	
$C_\alpha–C_m$	1.363 (8)	1.381 (2)	1.370 (6)	1.390 (6)	
bond angles (deg)					
N–M–N	90.1 (2)	89.9 (5)	90.0 (1)	88.8 (1)	
$M–N–C_\alpha$	128.0 (4)	*e*	*e*	126.7 (3)	decrease
$C_\alpha–N–C_\alpha$	104.1 (4)	105.0 (1)	105.5 (3)	106.4 (5)	increase
$N–C_\alpha–C_\beta$	110.8 (5)	111.0 (2)	110.2 (4)	110.1 (4)	
$C_\alpha–C_\beta–C_\beta$	107.2 (5)	106.5 (3)	107.1 (4)	106.7 (2)	
$N–C_\alpha–C_m$	124.4 (5)	124.5 (3)	124.2 (4)	124.3 (5)	
$C_\alpha–C_m–C_\alpha$	125.2 (4)	125.8 (5)	125.1 (4)	127.9 (3)	increase
$C_m–C_\alpha–C_\beta$	124.8 (5)	124.4 (3)	125.8 (4)	125.5 (3)	

[a] Data from ref 32. [b] Data from ref 58. $(3MePy)_2$ = bis(3-methylpyridine). [c] Data from ref 38. [d] Data from ref 59. [e] Not given in original paper.

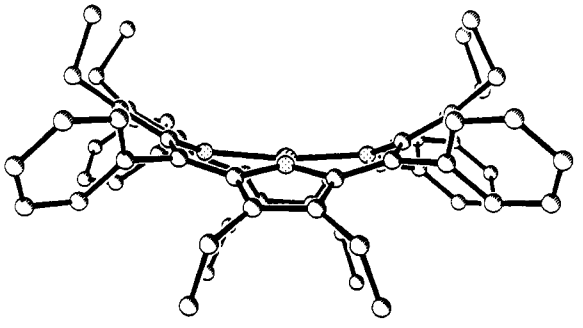

Figure 3. Side view of CuOETPP looking along the N–Cu–N axis.

scribed previously.[10] Nickel complexes of porphyrins **1**, **2**, and **6** were in saddle conformations while Ni porphine (NiP), NiOEP, NiTPP, and Ni **5** were essentially planar.

Results

X-ray Crystallography. The molecular structure and numbering scheme for CuOETPP is shown in Figure 2. The nonplanar saddle conformation of the CuOETPP molecule is best illustrated by the crystal structure view shown in Figure 3. The structures of CuOETPP and CoOETPP are similar to the crystal structure of $Zn(CH_3OH)$OETPP.[7] Selected bond lengths and angles for the Ni(II),[14] Co(II), Cu(II) and Zn(II)[7] complexes of OETPP and OEP are summarized in Tables III and IV, respectively. Additional structural parameters, including core size and out-of-plane displacements for metal complexes of OETPP, OEP, and TPP,

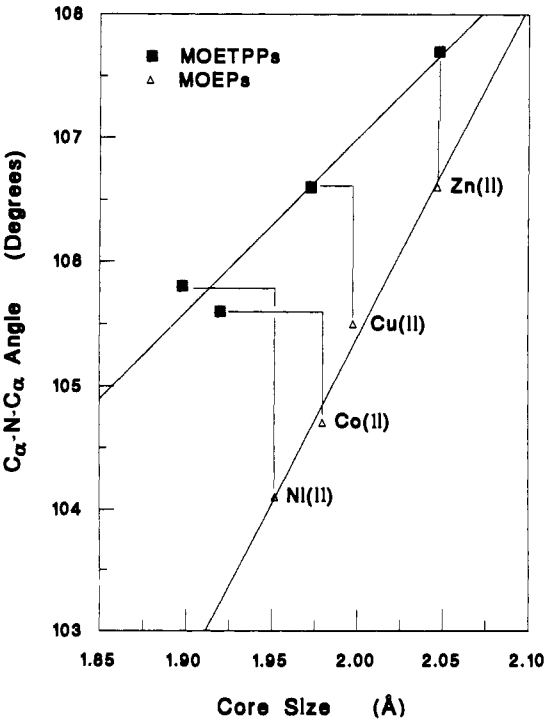

Figure 4. Plot showing the correlation between the $C_\alpha–N–C_\alpha$ angle and the core size, both from X-ray structural data, for MOEP and MOETPP complexes.

Table V. Selected Crystallographic and Calculated Structural Parameters of the Metal Octaethyltetraphenylporphyrins and of the Metal Octalkylporphyrins or Tetraarylporphyrins Used in Developing the Metal Force-Field Parameters

porphyrin	M–N bond (Å)	core size (Å)	$C_\alpha NC_\alpha$ angle (deg)	NMN angle[a] (deg)	twist angle[b] (deg)	RMS oop dev[c]	d_M[d] (Å)	d_N[d] (Å)	d_α[d] (Å)	d_β[d] (Å)	d_m[d] (Å)	RMS dev[e] (Å)
Crystallographic Parameters, MOETPPs												
NiOETPP[f]	1.906		105.9	168.7								
CoOETPP	1.929	1.920	105.6	170.0	2.7	0.732	0.018	0.176	0.472	1.168	0.053	
CuOETPP	1.977	1.973	106.6	172.0	2.6	0.700	0.004	0.137	0.439	1.125	0.041	
Zn(L)OETPP[g]	2.063	2.048	107.7	167.9	2.8	0.669	0.240	0.063	0.390	1.079	0.050	
Calculated Parameters, MOETPPs												
NiOETPP	1.903	1.878	106.1	161.3	7.8	0.771	0.000	0.313	0.492	1.221	0.017	*p*
CoOETPP	1.945	1.925	107.0	163.1	0.5	0.730	0.000	0.286	0.459	1.158	0.023	0.070
CuOETPP	1.966	1.947	107.5	164.2	0.6	0.709	0.000	0.272	0.442	1.125	0.025	0.088
Zn(L)OETPP[n]	2.066	2.058	109.7	170.1	3.8	0.612	0.060	0.177	0.357	0.985	0.066	0.107
NiOPTPP	1.903	1.880	106.1	161.5	8.6	0.764	0.001	0.308	0.483	1.202	0.152	*p*
$Co^{III}OETPP(L)_2$[o]	1.931	1.908	106.9	162.5	9.3	0.753	0.000	0.294	0.469	1.186	0.166	*p*
$Fe^{III}(Cl)OETPP$	1.971	1.971	107.6	164.7	0.6	0.701	0.005	0.263	0.435	1.116	0.018	*p*
Crystallographic Parameters, Planar Porphyrins												
NiOEP (tri B)[h]	1.952	1.952	104.1	180.0	0.8	0.029	0.000	0.011	0.016	0.030	0.032	
Co(L)TPP[i]	1.985	1.980	104.7	171.1	4.8	0.069	0.180	0.055	0.053	0.081	0.025	
CuOEP[j]	1.998	1.998	105.5	180.0	2.0	0.026	0.000	0.015	0.013	0.025	0.027	
Zn(py)TPyP[k]	2.073	2.047	106.6	161.7	0.8	0.091	0.369	0.045	0.033	0.145	0.010	
$Co^{III}(L)_2TPP$[l]	1.978	1.978	104.9	180.0	2.9	0.056	0.000	0.030	0.047	0.055	0.060	
$Fe^{III}(L)TPP$[m]	2.001	1.980	105.6	164.2	10.4	0.157	0.300	0.033	0.103	0.180	0.180	
Calculated Parameters, Planar Porphyrins												
NiOEP (tri B)	1.953	1.953	104.5	180.0	0.2	0.006	0.000	0.001	0.003	0.007	0.002	0.031
Co(L)TPP[q]	1.986	1.975	105.8	168.5	9.8	0.122	0.272	0.076	0.091	0.207	0.164	0.098
CuOEP	1.988	1.998	106.1	180.0	0.2	0.005	0.000	0.001	0.002	0.007	0.001	0.028
Zn(py)TPyP[r]	2.073	2.065	108.7	170.2	1.5	0.055	0.236	0.059	0.016	0.066	0.027	0.060
$Co^{III}(L)_2TPP$[s]	1.978	1.978	105.6	180.0	1.1	0.019	0.000	0.014	0.011	0.023	0.013	0.052
$Fe^{III}(L)TPP$[t]	2.001	2.000	106.4	176.8	2.0	0.023	0.074	0.033	0.014	0.022	0.007	0.163

[a] The N–M–N angle across the porphyrin (180° for a planar porphyrin) shows the degree of saddle-type distortion in the MOETPPs. [b] The twist of the pyrrole rings as defined by the C_α–N–N–C_α dihedral angle. [c] RMS out-of-plane deviation from the mean plane of the porphyrin consisting of the 24 C_β, C_α, C_m, and N atoms measured in Å. [d] Average out-of-plane displacement (*d*) of the metal (M), nitrogen (N), C_β (β), C_α (α), and C_m (m) atoms. Errors in the crystallographic out-of-plane displacements are less than 0.01 Å. [e] The RMS deviation for the best fit of the calculated structure to the corresponding X-ray structure for the C and N atoms of the macrocycle. [f] Data from ref 14a. [g] Data from ref 7. L = methanol. [h] Data from ref 32. [i] Data from ref 37, L = 1,2-dimethylimidazole. [j] Data from ref 38. [k] Data from ref 39. [l] Data from ref 40, L = piperidine. [m] Data from ref 41, L = $OClO_3$. [n] L = methanol. [o] L = pyridine. [p] Crystal structure not available for comparison. [q] L = 1,2-dimethylimidazole. [r] py = pyridine and TPyP = tetrapyridylporphyrin. [s] L = piperidine. [t] L = $OClO_3$.

are summarized in Table V. Figure 4 shows the correlations between the C_α–N–C_α angle and the core size for MOETPPs and MOEPs. Complete structural information for CuOETPP and CoOETPP obtained from X-ray crystallography, including the fractional atomic coordinates and equivalent isotropic displacement coefficients, is given in the supplementary material.

Molecular Mechanics Calculations. It was necessary to model known crystal structures of nearly planar porphyrins for the purpose of obtaining force field parameters for the metals. The structures chosen were the most planar ones that contained metals in the same oxidation and spin states as the metal OETPP complexes. The structures used to obtain the metal parameters were (1) nickel(II) octaethylporphyrin (triclinic B form),[32] NiOEP triB, (2) cobalt(II) (1,2-dimethylimidazole)tetraphenylporphyrin,[37] Co(1,2-Me_2Im)TPP, (3) copper(II) octaethylporphyrin (triclinic B form),[38] CuOEP triB, (4) zinc(II) tetra(4-pyridyl)porphyrin monopyridine,[39] Zn(py)TPyP, (5) cobalt(III) tetraphenylporphyrin cation bis-piperidine [NO_3^-, HCO_3^-],[40] $Co^{III}(pip)_2TPP^+$, and (6) iron(III) perchloratotetraphenylporphyrin,[41] $Fe^{III}(OClO_3)TPP$.

Structural parameters obtained from energy-optimization calculations for the MOETPP and MOEP complexes are given in Table V. Figure 5 shows the crystal (gray) and calculated (solid) structures of CuOETPP, where the two structures have been superimposed by least-squares matching the macrocyclic carbon and nitrogen atoms. The last column of Table V lists the root-mean-square (RMS) deviation for the best fit of the calculated structure to the corresponding X-ray structure for the carbon and nitrogen atoms of the macrocycle, an overall measure of the accuracy of the predicted conformation. The RMS out-of-plane deviation between predicted and experimental structures is gen-

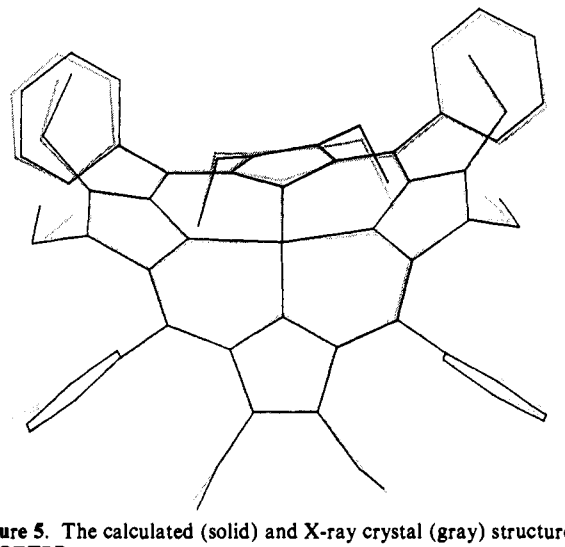

Figure 5. The calculated (solid) and X-ray crystal (gray) structures of CuOETPP.

(37) Dwyer, P. N.; Madura, P.; Scheidt, W. R. *J. Am. Chem. Soc.* **1974**, *96*, 4815–4819.
(38) Pak, R.; Scheidt, W. R. *Acta Crystallogr.* **1991**, *C47*, 431–433.
(39) Collins, D. M.; Hoard, J. L. *J. Am. Chem. Soc.* **1970**, *92*, 3761–3771.
(40) Scheidt, W. R.; Cunningham, J. A.; Hoard, J. L. *J. Am. Chem. Soc.* **1973**, *95*, 8289–8294.
(41) Reed, C. A.; Mashiko, T.; Bentley, S. P.; Kastner, M. E.; Scheidt, W. R.; Spartalian, K.; Lang, G. *J. Am. Chem. Soc.* **1979**, *101*, 2948–2958.

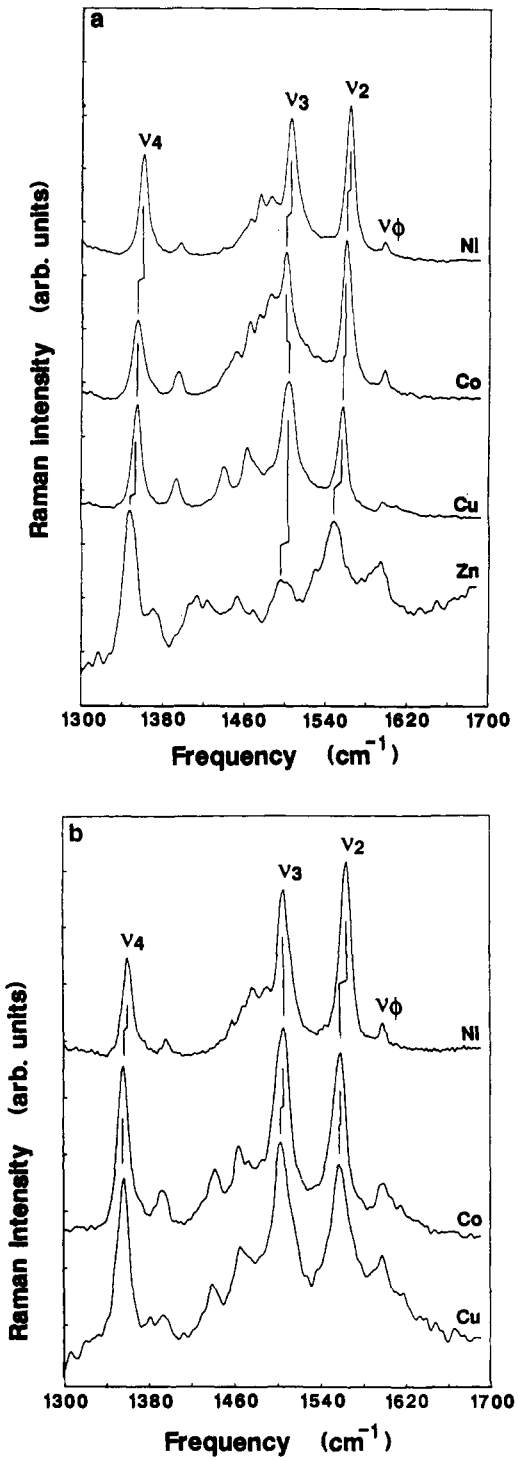

Figure 6. (a) Resonance Raman spectra of the MOETPPs in carbon disulfide. (b) Resonance Raman spectra of the MOETPPs in polycrystalline form. Laser excitation was 413.1 nm in both cases. Structure-sensitive lines are indicated.

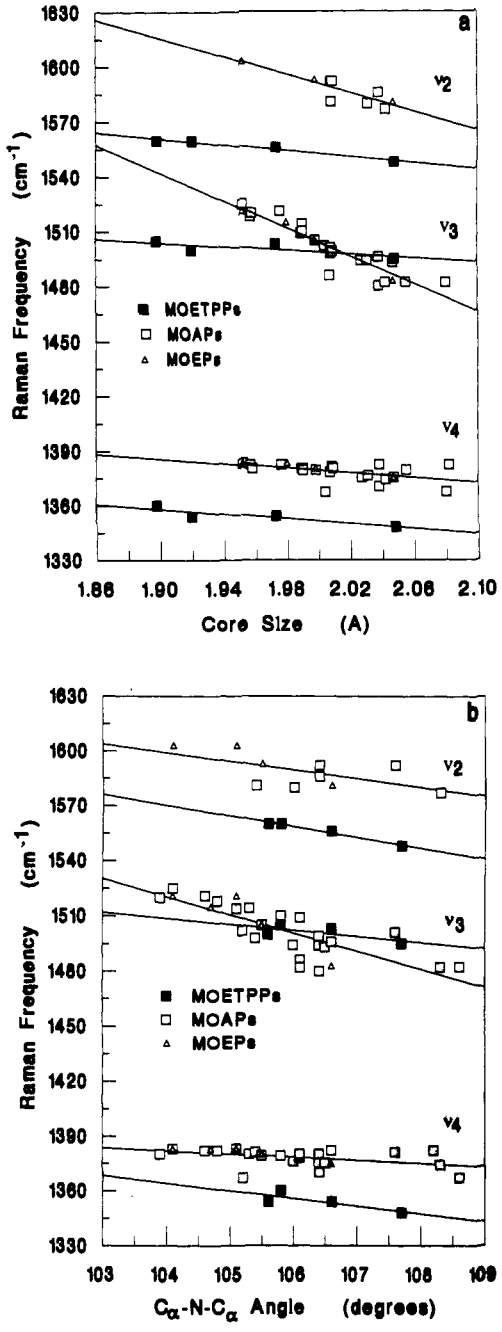

Figure 7. (a) Plot showing the relationship between the core size and Raman frequencies for the structure-sensitive marker lines, ν_4, ν_3, and ν_2, for the metal complexes of OAP (□), OEP (△), and OETPP (■). All points were taken from X-ray crystal data except that for NiTPP which was obtained via molecular mechanics calculations. (b) Plot showing the relationship between C_α–N–C_α angle and Raman frequencies for the structure-sensitive marker lines, ν_4, ν_3, and ν_2, for the same series of porphyrins as in part a.

erally less than 0.1 Å with the largest RMS deviations occurring for those porphyrins possessing axial ligands. The calculations generally underestimate the out-of-plane distance of the metal in these complexes (Table V). The core size given in the tables is defined as the length of the projection of the M–N bond into the average plane of the pyrrole nitrogens. If the pyrrole nitrogens are in the mean porphyrin plane, then this reduces to the center-to-nitrogen (Ct–N) distance which is usually quoted as the core size.

Resonance Raman Spectra of Metal Octaethyltetraphenylporphyrins. Figure 6 shows the solution (a) and polycrystalline (b) spectra of the MOETPPs in the region 1300–1700 cm^{-1}. Most of the structure-sensitive Raman lines including ν_4, ν_3, and ν_2 are within this spectral region. Table VI lists the Raman frequencies of these lines in the solution and polycrystalline spectra of metal complexes of OETPP, OEP, and TPP.[42] In the case of the MOETPPs, the frequencies of the structure-sensitive lines for the crystalline samples do not differ significantly from those of the solution samples, indicating that the macrocycle maintains a

(42) Table VI corrects one datum from an earlier study (ref 10): ν_3 for NiTPP is at 1470 cm^{-1} instead of 1505 cm^{-1} as stated. Stichternath, A.; Schweitzer-Stenner, R.; Dreybrodt, W.; Mak, R. S. W.; Li, X.-Y.; Sparks, L. D.; Shelnutt, J. A.; Medforth, C. J.; Smith, K. M. *J. Phys. Chem.*, submitted.

Table VI. Raman Frequencies (cm^{-1}) for the Metal Complexes of Octaethyltetraphenylporphyrin, Octaethylporphyrin, and Tetraphenylporphyrin

porphyrin	solvent	ν_4	ν_3	ν_{11}	ν_2	ν_{19}	ν_{10}	ν_ϕ
			MOETPP, Solution[a]					
NiOPTPP	CS_2	1360	1505		1560			1599
NiOETPP	CS_2	1360	1504		1563			1598
CoOETPP	CS_2	1354	1500		1560			1597
CuOETPP	CS_2	1354	1503		1556			1596
$Zn(CH_3OH)OETPP$	CS_2	1348	1495		1548			1594
$Co^{III}OETPP(py)_2X$[b]	CS_2[b]	1351	1497		1559			1596
$Fe^{III}(Cl)OETPP$	CS_2	*h*	1499		1548			1596
			MOETPP, Polycrystalline[a]					
NiOETPP		1360	1506		1565			1599
CoOETPP		1356	1506		1558			1599
CuOETPP		1356	1503		1557			1598
$Co^{III}OETPP(py)_2X$[b]		1354	1499		1559			1599
			MOEP[a]					
NiOEP	CS_2	1383	1521	1577	1603		1657	
CoOEP[c]	KBr	1383	1515			1601	1651	
CuOEP	CS_2	1380	1505	1570	1593		1639	
ZnOEP	CS_2	1375	1483	1559	1581		1640	
$Co^{III}(OH)(Im)OEP$[c]	KBr	1382	1514			1598	1649	
$Fe^{III}(Cl)OEP$[d]	CH_2Cl_2[d]	1374	1492	1557	1579		1628	
			MTPP[a]					
NiTPP[e]	KCl	1374	1470	1504	1572	1550	1594	1599
Co(2MeImH)TPP[f]		1363		1590	1563			
CuTPP[d]	CH_2Cl_2[d]	1365		1501	1562	1525	1582	1599
ZnTPP[g]	CS_2	1357		1494	1551		1585	1599
$Co^{III}(Cl)TPP$	CS_2	1368		1502	1567			1598
$Fe^{III}(Cl)TPP$[d]	CH_2Cl_2[d]	1363			1553			1598

[a] All metals are M(II) unless otherwise specified. CH_2Cl_2 = methylene chloride, CS_2 = carbon disulfide, KX = potassium halide pellet. [b] The bis pyridine (py) complex with the unknown (X) counterion. The solution spectrum of this porphyrin was obtained in CS_2 with a trace of pyridine. [c] Data from ref 20. Im = imidazole. [d] Data from ref 60. Solvent is CH_2Cl_2/0.1 TBAP (tetrabutylammonium perchlorate). [e] Data from the normal-mode analysis of Li et al., ref 61. [f] Data from ref 22. MeIm = methylimidazole. [g] Data from ref 62. [h] Raman assignment is uncertain.

solution conformation close to that observed in the crystal structure.

Additional Raman active modes are observed for the OETPP complexes because of the lowered symmetry of the porphyrin compared to planar systems and because both meso and β-pyrrole substituent modes are present. Assignments for the Raman active vibrations in NiOETPP in CS_2 were proposed in a previous study[10] and similar assignments based on the depolarization ratios have recently been proposed.[42]

Figure 7 shows some correlations between Raman frequencies of the structure-sensitive modes and two structural parameters, the core size (a) and the C_α–N–C_α angle (b). Comparison of the plots reveals that the MOETPP data cover a similar range of core sizes as the metal complexes of OEP and other porphyrins, but they cover a smaller range of values of the C_α–N–C_α angle. For the MOETPPs, the core size ranges from 1.89 to 2.05 Å (Δ = 0.16 Å), and the C_α–N–C_α angle ranges from 105.6° to 107.7° (Δ = 2.1°). On the other hand, the core sizes for the metal complexes of the tetra- or octa-substituted porphyrins extend from 1.92 to 2.08 Å (Δ = 0.15 Å), and the C_α–N–C_α angles range from 103.9° to 108.6° (Δ = 4.7°).

Molecular Orbital Calculations. The calculated energies of the frontier molecular orbitals of several planar and nonplanar nickel porphyrins are shown in Figure 8. The molecular orbitals are labeled using D_{4h} symmetry following the convention of the porphyrin literature. Molecular orbitals that are important in the configuration interaction (CI) include the $b_{2g}(d_{xy})$, $e_g(d_{xz},d_{yz})$, $a_{1g}(d_{z^2})$, $e_g(d_\pi$ mixed with $\pi)$, $a_{2u}(\pi)$, $a_{1u}(\pi)$, $e_g(\pi^*)$, and $b_{1g}(d_{x^2-y^2})$. The b_{1u} and $b_{2u}(\pi^*)$ orbitals are also significant, but because they only contributed to higher excited states (generally above 25 000 cm^{-1}) they are not shown. Other molecular orbitals that could be included in the CI calculations had a minimal effect on the calculated spectra. For the series of porphyrins shown, the energies of the nickel d_{z^2} and porphyrin $a_{1u}(\pi)$ and $e_g(\pi^*)$ orbitals remained fairly constant for all of the porphyrins (Figure 8). For NiOETPP, NiOMTPP, and $NiTC_6TPP$, their nonplanar conformation slightly destabilizes most of the porphyrin π orbitals and the other metal d orbitals.

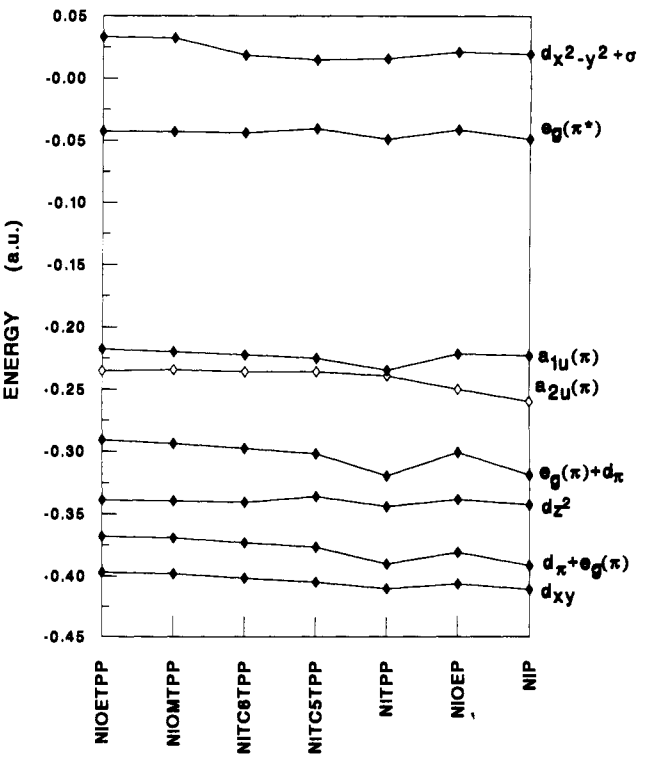

Figure 8. Plot showing the energies of the important molecular orbitals for nickel porphyrins calculated using INDO/CI.

Figure 9 shows the excited states calculated for the singlet (a) and triplet (b) manifolds. The calculated allowed $\pi \rightarrow \pi^*$ transitions to the Q and B singlet states are shown again in Figure 10 for comparison with the experimental values from the peaks

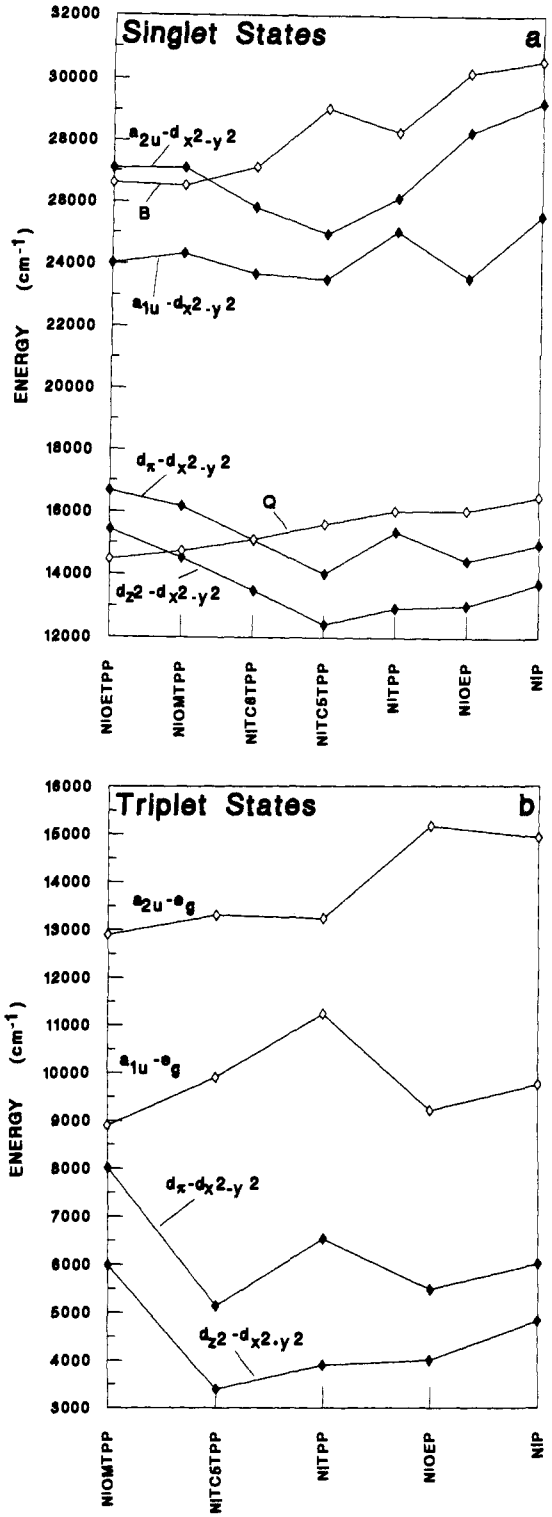

Figure 9. Plot showing the lowest energy singlet (a) and triplet (b) excited states for nickel porphyrins.

(λ_{max}) of the absorption bands (Soret, α, and β).

Discussion

Crystal Structures. It is known from crystallographic studies[43] that the porphyrin macrocycle is capable of accommodating metal ions of very different size. This appears to be achieved by a combination of (1) altering the bond angles and lengths of the porphyrin macrocycle and (2) changing the planarity of the

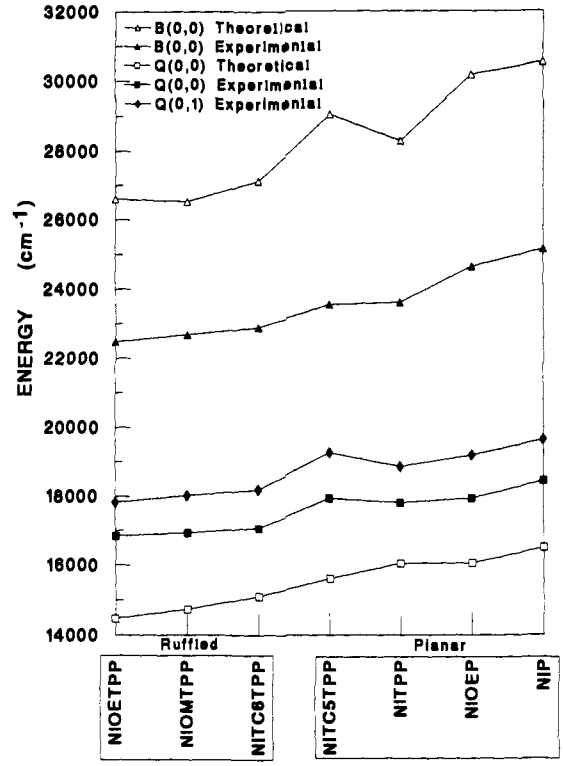

Figure 10. Plot showing the comparison of the calculated (INDO/CI) energies of the Q and B bands and the experimental transition energies for nickel porphyrins.

macrocycle. It is generally assumed that smaller metal ions such as nickel lead to less planar conformations than do larger metal ions,[43] although nonplanar conformations are frequently seen for large metal ions such as Pt,[44] In,[45] and Tl.[46] It was therefore not clear how the structures of porphyrins that are forced by severe steric strain to exist in nonplanar conformations would be affected by metal atoms of different size.

The crystallographic results obtained for the metal complexes of OETPP (Table V) show clearly that the metal atom alters the degree of planarity of the porphyrin macrocycle, with a larger metal atom favoring a more planar conformation. This is shown most clearly by the out-of-plane displacements (especially d_N, d_α, and d_β) given in Table V. The metals are listed in the order of their size as determined from either the van der Waals radius obtained from M–M distances in crystals of the pure metals (Ni, 1.25 Å; Co, 1.25 Å; Cu, 1.28 Å; Zn, 1.33 Å)[47] or the ionic radius (Ni, 0.69 Å; Co, 0.72 Å; Cu, 0.72 Å; Zn, 0.74 Å).[48] (The ionic radii of Fe(III) and Fe(II) are 0.64 and 0.74 Å, respectively, and that of Co(III) is 0.63 Å.[48]) However, the changes in macrocycle conformation are small for the MOETPP complexes, presumably because steric strain between the peripheral substituents inhibits flattening of the macrocycle.

The conformation of the MOETPPs, while being constrained to a highly nonplanar conformation, nevertheless responds to the metal size in a manner similar to unconstrained, planar porphyrins. This view is supported by the metal dependence of the bond lengths and bond angles for MOETPP and MOEP complexes summarized in Tables III and IV, respectively. In particular, similar trends in bonds and angles are observed for both planar and nonplanar porphyrins. Some of the changes in bond lengths and angles that

(43) (a) Hoard, J. L. In *Porphyrins and Metalloporphyrins*; Smith, K. M., Ed.; Elsevier: Amsterdam, 1975; Chapter 8. (b) Scheidt, W. R. In *The Porphyrins*; Dolphin, D., Ed.; Academic Press: New York, 1979; Vol. 3, Chapter 10.

(44) Hazell, A. *Acta Crystallogr.* **1984**, *C40*, 751–753.

(45) Ball, R. G.; Lee, K. M.; Marshall, A. G.; Troller, J. *Inorg. Chem.* **1980**, *19*, 1463–1469.

(46) Henrick, K.; Matthews, R. W.; Tasker, P. A. *Inorg. Chem.* **1977**, *16*, 3293–3298.

(47) *International Tables for X-ray Crystallography*; Birmingham: Kynoch Press (Present distributor Kluwer Academic Publishers: Dordrecht), 1962; Vol. III.

(48) *CRC Handbook of Chemistry and Physics*, 71 ed.; Lide, David R., Ed.; CRC Press: Boston, 1990.

occur for progressively larger metal atoms can readily be related to core expansion. (In this discussion we are excluding those bond lengths and bond angles obviously related to the metal atom because the metal out-of-plane displacement affects these parameters.) For example, the meso bridges open up (C_α–C_m–C_α angle increase) and elongate (C_α–C_m bond length increase). The core size is also increased by moving the pyrrole nitrogen further away from the metal atom, causing an increase in the C_α–N–C_α angle and a decrease in the N–C_α bond length. Other changes in bond lengths and angles are also observed and are consistent for both planar and nonplanar porphyrin complexes. These changes are small (generally less than 0.01 Å or 1° between the smallest and largest metal atoms studied) but are clearly related to the size of the metal core.

It is not surprising then that most of the changes in bond lengths and angles can be related to the size of the porphyrinato core. For example, Figure 4 shows the correlation between the C_α–N–C_α angles and core sizes obtained from the X-ray data for the metal series. The C_α–N–C_α angle for the nonplanar MOETPPs is consistently larger than that for the corresponding planar MOEPs. Because the core size is always smaller for a MOETPP than for the corresponding MOEP, it is also clear that nonplanar porphyrins prefer a smaller core than do planar porphyrins. A weaker dependence on core size (smaller slope) is also noted for the MOETPPs compared to the MOEPs. When a large metal (Zn) is put into the porphyrin, little core contraction is apparently possible for either the OEP or OETPP. The core contraction for the nonplanar MOETPPs relative to the MOEPs increases for the smaller metals (0.054 Å for Ni(II) as opposed to 0.001 Å for Zn(II)), as can be seen in Figure 4. The preference of the OETPP macrocycle for a smaller core size than the OEP macrocycle helps explain why large metals like Zn are easily lost from the OETPP complexes.[7]

Finally, the X-ray crystal structures of CoOETPP (not shown) and CuOETPP show a dichloromethane molecule in one of the two cavities formed by the axially-oriented ethyl groups. A second dichloromethane molecule observed in the crystal is located near one end of the cavity. The cavity on the other face of the macrocycle is occupied by the ethyl groups of another OETPP molecule. It is interesting to speculate on the effect that the cavity might have on the activity and selectivity of catalytic reactions occurring at the metal center.

Comparison of Calculated Structures and X-ray Crystal Structures. The ability to accurately calculate porphyrin geometry would be useful for investigations of protein–porphyrin interactions and for catalyst design. The molecular mechanics force field that we have used has been shown to accurately predict the macrocycle geometry for several nickel porphyrins including the most distorted case of Ni 3.[10] The accuracy of the force field in predicting the structures of other MOETPPs is shown by the close match of the experimental and calculated structures for CuOETPP in Figure 5 and by the RMS deviations for the nitrogen and carbon atoms of the macrocycle (last column, Table V). The average of the differences between the experimental and calculated OETPP values for the M–N distance, core size, and C_α–N–C_α angle is only 0.009 Å, 0.013 Å, and 1.2°, respectively, only slightly higher than the averages for the MOEPs and MTPPs (core size = 0.009 Å; C_α–N–C_α angle = 1.0°).

The calculated conformations obtained for the MOEPs, MTPPs (or MTPyP), and MOETPPs show many of the same trends that are observed in the experimental structures, despite the fact that only the metal parameters were modified. For example the C_α–N–C_α and C_α–C_m–C_α angles open up and the core size increases upon insertion of progressively larger metal atoms (Tables III and IV). Also, the C_α–C_m and C_β–C_β bond distances increase by 0.01 Å as the metal size increases (Ni to Zn). Other metal-dependent trends in macrocycle conformations of the MOETPPs are successfully predicted, including the flattening of the macrocycle for large metals.

There are notable structural differences between metal core geometries of the four- and six-coordinate metalloporphyrins and the five-coordinate porphyrin complexes. For example, the N–M–N angle is generally smaller and the out-of-plane displacement of the metal atoms is larger for the five-coordinate porphyrins than for the four- and six-coordinate porphyrins. This can be seen in both the calculated and the observed N–M–N angle and metal displacement (d_M, Table V). However, these values are poorly predicted by the calculations for the five-coordinate porphyrins. Thus, the metalloporphyrins that possess one axial ligand (Co(II), Zn(II), and Fe(III)) generally have higher RMS deviations from the crystal structure. Clearly, the force field parameters that determine the out-of-plane movement of the metal atom need to be improved.

Relationships between Raman Frequencies and Structural Parameters. The metal dependence of the Raman line frequencies for the MOETPP complexes provides a new opportunity to further characterize the relationships between Raman line frequencies and various structural parameters. Figure 6a and Table VI show that changing the metal has a small but significant effect on the solution Raman spectrum. In particular, the structure-sensitive Raman modes ν_4, ν_3, and ν_2 all shift to lower frequency (9–15 cm^{-1}) as the metal size increases in the series Ni, Co, Cu, and Zn. The major contribution to each of these modes is the C_α–N stretch for ν_4, the C_α–C_m stretch for ν_3, and the C_β–C_β stretch for ν_2.[31] The Raman shifts reflect the changes in these bond lengths with metal size. The range of variation in the latter two structure-sensitive marker lines (e.g., ν_2: 15 cm^{-1}) for the MOETPPs is smaller than that for the MOEPs (22 cm^{-1}) and MTPPs (21 cm^{-1}). (This difference in variation with core size is also evident in the slopes of the correlations in Figure 7a.)

The correlation between the frequency of the structure-sensitive Raman lines and the core size is largely coincidental in that the correlation relies on the structural relationship between core size and the bonds (force constants) that contribute to the Raman modes. Moreover, the structural relationship between core size and bond length may also depend on the type of perturbation that causes the change in core size. For example, both distortion from planarity and variation in metal size cause changes in core size, but the resulting structural relationships between bond lengths and core size may differ for these two perturbations, leading to different frequency–core size correlations. This was found to be the case in a previous investigation of distorted NiOATPPs.[10,21] The different frequency correlations observed for the series of NiOATPPs clearly indicate that core size is not the determining factor for the marker line frequencies. While the conventional core size correlation breaks down in the case of nonplanar distortion, similar linear correlations were found for another parameter, the C_α–N–C_α angle.[10,21] The C_α–N–C_α angle correlation, which gave similar negative slopes for both the metal–octaalkylporphyrin (MOAP) and NiOATPP data sets, also relies on coincidental structural relationships between the C_α–N–C_α angle and the bonds that contribute to the structure-sensitive modes. The success of the C_α–N–C_α angle–frequency correlation may result from the close relationship between this angle and the bonds contributing to the marker lines.

The Raman and X-ray data of this study extend the previous arguments concerning the C_α–N–C_α angle. In Figure 7, least-squares fits are shown for the Raman frequencies versus core size (a) and C_α–N–C_α angle (b) for both MOEPs and MOETPPs. Previous data for the MOAPs and our data for some MOEPs were fit with one line. The slopes of the linear estimates for ν_2 and ν_3 for the core size plots (Figure 7a) indicate much less dependence on core size for MOETPP complexes (–83 and –53 cm^{-1}/Å) than for the MOEP complexes (–250 and –381 cm^{-1}/Å). The large range of core sizes for the MOETPPs ensures that the weak dependence for the MOETPP complexes is not an artifact of the small data set (four points). Thus, yet another correlation between Raman frequency and core size is observed for the MOETPPs. The new correlation that is observed for the metal complexes of nonplanar OETPP is probably a result of a different structural relationship between core size and the bonds that contribute to the structure-sensitive modes. This probably results from the nonplanarity. (However, one must keep in mind that the relative contribution of the force constants to the modes can also vary.)

For the C_α–N–C_α angle plots (Figure 7b), the slopes of the linear estimates for ν_2 and ν_4 indicate that these modes depend on the C_α–N–C_α angle in similar ways for the MOEPs/MTPPs and the MOETPPs. However, our confidence in the slopes of the best fit lines for ν_3, ν_2, and ν_4 in the C_α–N–C_α angle plots is not as great as for the core size plots because the MOETPPs cover only a small range of C_α–N–C_α angles and only a small number of data points are available.[49] Vertical shifts of the MOAPs and MOEPs ($\sim$20 cm^{-1} with respect to the MOETPPs) for ν_2 and ν_4 for both the core size and C_α–N–C_α angle correlations are also noted. Previously, such shifts were noted between the correlation for the MOAPs and MTPPs.[50]

Considering the whole body of Raman data, which now includes both nonplanar and planar porphyrins containing different metals, we must conclude that core size is not the structural parameter that determines the frequency of the structure-sensitive Raman lines. The reason for this conclusion is that the slopes of the correlations are different depending on the porphyrin series, e.g., positive slopes for a series of progressively more distorted nickel porphyrins, small negative slopes for the nonplanar OETPP metal series, and large negative slopes for the planar MOEPs. One consequence of these differing correlations is that the core size correlations cannot be applied in the absence of additional structural information on planarity. On the other hand, the C_α–N–C_α angle is still a candidate for a more direct factor in modulating the force constants that provide the major contributions to the structure-sensitive normal modes.

Molecular Orbital Calculations (INDO/CI). The calculated lowest energy excited states (singlets and triplets) for the nickel porphyrins are shown in Figure 9. Low-energy transitions in the singlet manifold give rise to the Q and B states observed as the UV–visible absorption bands. These are CI mixtures of the $a_{1u} \rightarrow e_g$ and $a_{2u} \rightarrow e_g$ transitions.[51] Figure 10 shows a plot of the calculated energies of the Q and B states and the experimental transition energies, given by the peaks (λ_{max}) of the Q and B absorptions. The trends in the series (i.e. the shifts in absorption band energies for different porphyrins) are predicted fairly accurately, although the Q(0,0) band is consistently predicted to be about 2000 $\pm$ 400 cm^{-1} low and the B band is consistently predicted to be 4500 $\pm$ 1000 cm^{-1} high.

The triplet spectrum includes the $^3T_1(a_{1u} \rightarrow e_g)$ and $^3T_2(a_{2u} \rightarrow e_g)$ $\pi \rightarrow \pi^*$ states. In addition, photoexcitation of Ni porphyrins in noncoordinating solvents produces[51,52] an excited state that decays to the $^1A_{1g}$ ground state in about 300 ps. On the basis of the transient absorption and resonance Raman spectra, this state is a low-lying d–d excited state.[51-53] The calculations indicate that the $^3B_{1g}(d_{z^2} \rightarrow d_{x^2-y^2})$ is the lowest calculated state for all the porphyrins in this series. Thus the calculations and the experimental results agree that the excited state is the $^3B_{1g}$.

The energies of the d–d transitions show a dependence on the Ni–N distance which may partly explain why axial coordination does not occur for the saddle shaped nickel porphyrins investigated so far.[13] The $^3B_{1g}$ state rises significantly in energy (almost 0.5 eV) as the Ni–N distance becomes smaller and the porphyrin macrocycle more nonplanar (Figure 9). Upon axial ligation, an electron must be promoted in order to leave a half-empty d_{z^2} orbital to accept charge from the lone pair of the coordinating base. By raising the energy of the $^3B_{1g}(d_{z^2} \rightarrow d_{x^2-y^2})$ state (the ground state when a ligand is bound), the nonplanarity effectively lowers the ligand affinity. Nonplanarity has been suggested to play a role in determining the ligand affinity of isomers of cofactor F_{430} of methylreductase.[54-56]

Other low-energy d–d transitions include $d_\pi \rightarrow d_{x^2-y^2}$ and $d_{xy} \rightarrow d_{x^2-y^2}$. The $d_{xy} \rightarrow d_{x^2-y^2}$ transition was not calculated because the d_{xy} orbital is so low in energy that the program did not include it in the CI calculations. The low-lying charge-transfer transitions include $a_{1u} \rightarrow d_{x^2-y^2}$ and $a_{2u} \rightarrow d_{x^2-y^2}$.

The most important finding of the MO calculations is that a combination of the molecular mechanics and INDO/CI calculations can accurately predict trends in the $\pi \rightarrow \pi^*$ transition energies for nickel porphyrins. However, in many molecular orbital calculations of porphyrin spectra, planar porphyrin structures are used and the correct peripheral substituents are not included, i.e., hydrogens are generally used in place of the actual substituents in order to simplify the calculations. Our MO calculations using the calculated Ni porphyrin structure but with hydrogens in place of the substituents revealed that the correct substituents need to be included in order to obtain good agreement with the spectral trends for this series of porphyrins. The substituents have as large of an effect on the transition energies as the distortion of the macrocycle. In fact, using an incorrect (planar) porphyrin geometry in the MO calculations even with the correct substituents gives poor agreement with the absorption spectra. The success of the INDO/CI calculations using the structures obtained from molecular mechanics calculations shows that these structures must be a reasonable approximation to the structure in solution. Thus, the INDO/CI method, used in combination with structures predicted by the molecular mechanics calculations, is one way to accurately predict the effects of both the macrocycle conformation and the substituents on the $\pi \rightarrow \pi^*$ transition energies of porphyrins.

Conclusions

A comparison of structures obtained from X-ray crystallographic data and molecular mechanics calculations suggests that reasonably accurate predictions of metalloporphyrin structures can be made. Many trends in the structural parameters (bond length, bond angles, out-of-plane displacements, core size, etc.) resulting from an increase in the metal size can be accurately predicted by molecular mechanics calculations. Of particular interest is the fact that the decrease in nonplanarity of the MOETPPs because the metal size increases is successfully predicted. This is especially encouraging as the force field is based on planar porphyrins that are not sterically constrained, and yet it accurately predicts the structural trends observed in the nonplanar sterically-crowded porphyrins.

Also of interest is the metal dependence of potential substrate binding pockets in highly distorted porphyrins such as the MOETPPs. Both X-ray crystallography and molecular mechanics calculations show that as the size of the metal increases, the cavity formed by the ethyl groups of MOETPP opens up due to a flattening of the macrocycle. It is interesting to note that a dichloromethane molecule is located in this cavity in the Co and CuOETPP crystals. Dichloromethane is a good analog for other small substrate molecules such as carbon dioxide in that it possesses similar size and partial atomic charges. The calculated binding energies for a series of small substrate molecules including methane, carbon dioxide, dichloromethane, and others have been found to decrease as the pocket opens up for large metals.[57]

The relationships among various structural parameters and the frequencies of the structure-sensitive Raman modes are consid-

(49) For the C_α–N–C_α angle dependence for ν_3 of the MOETPPs there are only four data points and the scatter in the data is apparently slightly greater than for the MOAP/MOEP data. Therefore, the slope of the best fit line for ν_3 may be incorrect and the C_α–N–C_α angle dependence may not be representative of a broader range of data.

(50) Spiro, T. G. In *Iron Porphyrins*; Lever, A. B. P., Gray, H. B., Eds.; Addison-Wesley: Reading, 1983; Chapter 3.

(51) Gouterman, M. *J. Chem. Phys.* **1959**, *30*, 1139–1161.

(52) Kim, D.; Kirmaier, C.; Holten, D. *Chem. Phys.* **1983**, *75*, 305–322.

(53) Findsen, E. W.; Shelnutt, J. A.; Ondrias, M. R. *J. Phys. Chem.* **1988**, *92*, 307–314.

(54) Eschenmoser, A. *Ann. N.Y. Acad. Sci.* **1986**, *471*, 108–128.

(55) Shiemke, A. K.; Shelnutt, J. A.; Scott, R. A. *J. Biol. Chem.* **1989**, *264*, 11236–11245.

(56) Shiemke, A. K.; Kaplan, W. A.; Hamilton, C. L.; Shelnutt, J. A.; Scott, R. A. *J. Biol. Chem.* **1989**, *264*, 7276–7284.

(57) Shelnutt, J. A.; Hobbs, J. D. *ACS Fuel Div. Prepr.* **1992**, *37*, 332–339.

(58) Little, R. G.; Ibers, J. A. *J. Am. Chem. Soc.* **1974**, *96*, 4440–4446.

(59) Cullen, D. L.; Meyer, E. F., Jr. *Acta Crystallogr.* **1976**, *B32*, 2259–2269.

(60) Czernuszewicz, R. S.; Macor, K. A.; Li, X.-Y.; Kincaid, J. R.; Spiro, T. G. *J. Am. Chem. Soc.* **1989**, *111*, 3860–3869.

(61) Li, X.-Y.; Czernuszewicz, R. S.; Kincaid, J. R.; Su, Y. O.; Spiro, T. G. *J. Phys. Chem.* **1990**, *94*, 31–47.

(62) Walters, V. A.; dePaula, J. C.; Babcock, G. T.; Leroi, G. E. *J. Am. Chem. Soc.* **1989**, *111*, 8300–8302.

erably modified for the nonplanar MOETPPs in comparison with planar MOEP and MTPP counterparts. In particular, the dependence of ν_2 and ν_3 on core size is greatly decreased for the nonplanar porphyrins. Such spectral relationships are often useful in structure–function correlations in molecular biology and play a central role in the use of Raman spectroscopy in studies of the chemical and photochemical function of tetrapyrrole cofactors in proteins and in other chemical environments. Relationships among the frequencies of structure-sensitive Raman lines and two structural parameters, porphyrin core size and C_α–N–C_α angle, have been analyzed for the MOETPP series. The MOETPPs show only weak variation in Raman frequencies in spite of large differences in core size (0.15 Å) for the series of metals employed. This behavior contrasts sharply with those of the metal TPPs and OEPs which exhibited a strong metal dependence over this range of core sizes. On this basis core size does not determine the frequency of the structure-sensitive Raman lines. On the other hand, the frequency dependence on the C_α–N–C_α angle, which varies only over a small range (2°) for the MOETPPs, is comparable (within the uncertainties in the slope) to that for the MOAPs.

Porphyrin optical transitions are also affected by deviations from planarity. INDO/CI molecular orbital calculations can accurately predict the trends in the $\pi \rightarrow \pi^*$ transitions for a series of nickel porphyrins with varying nonplanarity if the structures obtained from molecular mechanics are used in the MO calculations. However, accurate prediction of the transition energies also requires the inclusion of all macrocycle substituents in the MO calculations.

In summary, the results presented here and elsewhere demonstrate that molecular mechanics calculations can be used to predict the structures of highly substituted porphyrins, including the structural effects of different substituents and metal ions and the degree of nonplanarity[9-11] and the type of nonplanar distortion.[14b] Clear relationships are observed between the metal present in the porphyrin and structural parameters determined by resonance Raman, optical absorption, and NMR spectroscopy.[7,9-11,14] This information is currently being used in the molecular design of nonplanar pocket porphyrins as biomimetic catalysts.

Acknowledgment. We thank K. M. Barkigia and J. Fajer for communicating their results for the X-ray crystal structure of NiOETPP prior to publication. Work performed at Sandia National Laboratories was supported by the U.S. Department of Energy Contract DE-AC04-76DP00789 (J.A.S.). Work performed at the University of California was supported by the National Science Foundation Grant CHE-90-01381 (K.M.S.) and the Deutsche Forschungsgemeinshaft Se 543/1-1 (M.O.S.). C.J.M. thanks the Fulbright Commission for the award of a Travel Scholarship and L.D.S. thanks the Associated Western Universities for a Graduate Fellowship.

Supplementary Material Available: Labeling scheme for CoOETPP and details of the crystal structure determinations of CoOETPP and CuOETPP including lists of atomic coordinates, anisotropic thermal parameters, H-atom coordinates, bond lengths, bond angles, torsion angles, and least-squares planes (31 pages); listing of observed and calculated structure factors (88 pages). Ordering information is given on any current masthead page.

Chemical and Electrochemical Investigation of Redox-Associated Conformational Changes in the Bis(1,4,7-trithiacyclononane)copper(II/I) System and X-ray Structure of the Copper(I) Complex

Sanaullah, Kenji Kano,[†] Richard S. Glass,[‡] and George S. Wilson*

Contribution from the Department of Chemistry, The University of Kansas, Lawrence, Kansas 66045. *Received July 15, 1992*

Abstract: Extensive electrochemical measurements of the kinetic parameters for electron transfer in aqueous bis(1,4,7-trithiacyclononane)copper(II) ($[Cu^{II}(TTCN)_2]$) and its Cu(I) analog have been carried out at a glassy carbon electrode. Our studies have shown that the $[Cu^{II}(TTCN)_2]/[Cu^{I}(TTCN)_2]$ system follows an ECEC square mechanism rather than just simple electron transfer as suggested previously. Unlike the octahedral Cu(II) complex, $[Cu(TTCN)_2]PF_6$ crystallizes with two independent formula units in space group $P2_1/n$ of the monoclinic system with unit cell dimensions a = 8.608 (3) Å, b = 31.041 (8) Å, c = 16.008 (4) Å, and β = 90.88 (2)°. The two molecular units have distorted tetrahedral CuS_4 coordination spheres with monodentate and tridentate TTCN ligands. The mondentate ligands have a unique conformation for the TTCN moiety with Cu(I) coordinated differently in each of the two independent $[Cu^{I}(TTCN)_2]$ units. The ring conformation, however, remains the same. The uncoordinated sulfur atoms on the monodentate TTCN ligand can coordinate to a metal ion added to the solution, and this ligand ultimately reverts to a tridentate ligand with the standard endodentate [3 3 3] conformation of the TTCN moiety. The transient trinuclear complex with added Cu(II) can be detected both electrochemically and spectrophotometrically. Electrochemical oxidation of $[Cu^{I}(TTCN)_2]$ and reduction of $[Cu^{II}(TTCN)_2]$ both occur rapidly, but in both cases, the electron transfer is followed by chemical steps. These chemical steps are the conformational reorganization of the monodentate TTCN ligand into the tridentate [3 3 3] conformer and the reverse of this process, respectively. Digital simulations of the cyclic voltammetric data for the kinetic parameters of both the $[Cu^{II}(TTCN)_2]/[Cu^{I}(TTCN)_2]$ system and the entire mechanism of the interaction between $[Cu^{I}(TTCN)_2]$ and Cu(II) followed by the subsequent reduction of the intermediate have been carried out.

Introduction

Despite the significantly different coordination geometries of Cu(II) and Cu(I) cations, a number of copper proteins involved in electron transport in biological systems accommodate these differences. This has inspired research directed toward characterization of the metal center. The facile electron transfer in these proteins has been accomplished (i) by geometrical preorganization of the metal-binding site in a near-entatic state and (ii) by an exquisite selection of the ligand system about the metal center such that both the oxidized and reduced states will be stabilized.[1]

[†] Gifu Pharmaceutical University, 5-6-1 Mitahora-Higashi, Gifu 502, Japan.
[‡] Department of Chemistry, The University of Arizona, Tucson, AZ 85721.

(1) Colman, P. M.; Freeman, H. C.; Guss, J. M.; Murata, M.; Norris, V. A.; Ramshaw, J. A. M.; Venkatappa, M. P. *Nature (London)* **1978**, *272*, 319.

0002-7863/93/1515-592$04.00/0